

RESEARCH ARTICLE

Non-linear ultimate strength and stability limit state analysis of a wind turbine bladeMalo Rosemeier¹, Peter Berring² and Kim Branner²¹ Division Structural Components, Fraunhofer Institute for Wind Energy and Energy System Technology IWES, Am Seedeich 45, 28572 Bremerhaven, Germany² Department of Wind Energy, Technical University of Denmark, Frederiksborgvej 399, Roskilde 4000, Denmark**ABSTRACT**

According to the design codes for wind turbine blades, it is sufficient to evaluate the blade's limit states using solely a linear analysis. This study, however, shows the need of non-linear analyses in blade design. Therefore, a geometrically non-linear structural response of a 34 m blade under flap-wise loading has been compared with a linear response to determine the blade's resistance in the ultimate strength and stability limit states. The linear analysis revealed an unrealistic failure mechanism and failure mode. Further, it did not capture the highly non-linear response of the blade that was measured in an ultimate full-scale test to failure and determined by a geometrically non-linear analysis. A design evaluation in accordance with the least stringent Germanischer Lloyd (GL) requirements has been compared with non-linear approaches proposed by GL and Eurocode, which require the application of an imperfection. The more realistic non-linear approaches yielded more optimistic results than the mandatory linear bifurcation analysis. Consequently, the investigated blade designed after the lesser requirements was sufficient. Using the non-linear approaches, considering inter-fibre failure as the critical failure mode, yielded still a significant safety margin for the designer (7–28%). The non-linear response was significantly dependent on the scaling of the imperfection. Eurocode's method of applying an imperfection appeared more realistic than the GL method. Since the considered blade withstood 135% of the design load at a full-scale test to failure and the blade has operated successfully in the field, GL's safety factors combined with the imperfection size may be too conservative. Copyright © 2015 John Wiley & Sons, Ltd.

KEYWORDS

ultimate limit state; blade design; certification; stability; buckling; strength; Germanischer Lloyd; Eurocode

Correspondence

Malo Rosemeier, Division Structural Components, Fraunhofer Institute for Wind Energy and Energy System Technology IWES, Am Seedeich 45, 28572 Bremerhaven, Germany.

E-mail: malo.rosemeier@iwes.fraunhofer.de

Received 18 September 2014; Revised 7 April 2015; Accepted 16 May 2015

NOMENCLATURE

l_B	blade length measured from the root	l_g	relevant dimple length
F	internal load	U_0	dimple tolerance factor
γ_r	safety factor for loads	\mathbf{K}	stiffness matrix
f	material property	λ	eigenvalue
γ_m	safety factor for material	Φ	eigenvector
γ_n	safety factor for consequence of failure	u	displacement
S	load effect	σ, τ	stress
R	resistance, strength	FI	failure index
SRF	safety reserve factor	Index m	mean
MoS	margin of safety	Index k	characteristic
P_d	external load at the design point		

P_f	external load at failure	Index G	geometric
P_{cr}	buckling resistance	Index \parallel	parallel to fibre axis orientation
a	geometrical parameters	Index \perp	perpendicular to fibre axis orientation
Δw_0	dimple amplitude		

1. INTRODUCTION

Both linear and non-linear finite element (FE) analyses are used by engineers to investigate the structural response of a rotor blade. A linear analysis (LA) underlies the simplification that the loading conditions in a blade are deformation independent. The independence of deformation in LAs is restricted by the presumption of small displacements and small angles. In contrast, the deformation history of a non-linear analysis is a function of load. When the non-linearity is caused by the change of structural shape, this characteristic is defined as geometric non-linearity. Thin-walled structures—such as wind turbine blades—show geometrically non-linear responses, i.e. buckling, cross-sectional warping or the flattening of the cap due to the Brazier effect¹ as investigated by Cecchini and Weaver² and Jensen *et al.*³ These responses are also caused by the blade's curved, tapered and twisted geometry as well as the high Poisson's ratios of the materials used in a design. These effects, however, are not taken into account when considering an LA.

Two studies compare linear with geometrically non-linear analyses (GNAs): a relatively coarse meshed FE model of a 24 m wind turbine blade was validated with a full-scale test at design loading conditions in Kong *et al.*⁴ For the considered structural responses—where the strain level is also very low—an LA gives good agreement with the test. This indicates that geometrically non-linear effects are not significant for this particular design. However, geometric non-linearity is more dominant at a larger load level above design load, which has not been investigated. The 34 m blade considered in this study was tested in a full-scale test to failure in Jensen *et al.*⁵ Further, the relative deflection of the caps was compared with an LA and a GNA. The cap's structural response was significantly non-linear. Basically, it has been argued that the Brazier effect is the dominant failure mechanism for structural collapse. It is recommended to use global geometrically non-linear FE analyses in the design process.

Numerous flap-wise full-scale tests to failure showed that geometrically non-linear effects dominate the failure mechanism: a 25 m blade was tested to failure in Jørgensen *et al.*⁶ Strain gauge measurements and local deflections of the cap under compression indicated local geometrically non-linear behaviour. Another 25 m blade was tested to failure and validated with GNA in Overgaard *et al.*⁷ and Overgaard and Lund.⁸ It was found that the suction side cap deflects in a global manner, and it collapses because of geometrically non-linear local buckling and delamination instead of the Brazier effect. A 40 m blade was tested to failure at 160% of its design load and compared with GNA in Yang *et al.*⁹ The structural collapse was caused by debonding of the aerodynamic shell amplified by local buckling and delamination. In Chen *et al.*,¹⁰ GNA of a 52.3 m blade were validated against a test to failure. Local out-of-plane deformation of the cap was caused by local buckling, while the Brazier effect was not responsible for the failure.

Predicting the strength of adhesive joints in wind turbine blades is important for the design of such blades. A practical approach to fracture analysis at the trailing edge of wind turbine blades is presented in Eder *et al.*¹¹ based on a linear fracture mechanics analysis. In Eder and Bitsche,¹² the influence of geometrical non-linearity in form of local buckling is studied. It is found that local buckling induces a significant increase of the energy release rate and also a change of mode mixity in the trailing edge joint. Thus, to reliably predict the strength of adhesive joints, the use of GNA is also important.

To the authors' knowledge, the effect of using linear and geometrically non-linear FE methods in certification of a real wind turbine blade is published in open literature for the first time in this paper. The analyses and discussion of the effect of geometric imperfections in the framework of certification of wind turbine blades are also new to the authors' knowledge. The findings in this paper put current standards and practices in certification of wind turbine blades into serious question.

In order to critically evaluate current certification practices, we study the answers to four questions. We analysed the response of a wind turbine blade in detail with both linear and GNA methods and answer the first question:

1. Do we need a GNA method in wind turbine blade design?

To obtain a permit for erecting a wind turbine, a manufacturer requires a certificate for its design. A certification body issues a certificate when a blade design fulfils the requirements according to standards and guidelines. The Germanischer Lloyd (GL) guideline¹³ describes as least stringent, most conservative requirement that an LA for the validation of the ultimate limit states: strength and stability. Further, validation via a geometrically non-linear approach is also possible but not mandatory. We investigated both validation methods and answer a second question:

2. Does the linear GL approach reveal more conservative results than the geometrically non-linear GL approach?

Wind turbine rotor blades are thin-walled composite structures. Assuming similar behaviour to thin-walled steel structures, those structures are highly sensitive to geometric imperfections.¹⁴ Imperfections have to be considered because real blades that depart the manufacturer's mould are never perfect. Because of manufacturing uncertainties, small dimples on

the surface or variations in wall thickness may occur. Thin-walled steel structures are designed according to Eurocode standard.¹⁵ This standard is specific for cylindrical shells and based on empirical investigations. Compared with GL's approach, Eurocode contains a more extended analysis method for the evaluation of the geometrically non-linear stability limit state. We compare both methods and answer a third question:

3. Is Eurocode's more extended geometrically non-linear stability analysis method more realistic than GL's method?

Comparing the requirements for the application of imperfections in both, GL guideline and Eurocode, the second contains more detailed requirements. Thus, we applied an imperfection on a blade model according to both requirements and answer a fourth question:

4. How realistic is the GL approach to apply an imperfection in comparison with Eurocode's approach?

Non-LAs are usually conducted as numerical FE analyses. Computational costs for non-LA depend on the degree of detail and the size of the model, whereas cost for LA is relatively low. For a long time, the computing requirements of non-linear approaches precluded their use. Nowadays, computational costs have decreased, and the computational power has risen. Therefore, engineers use non-LA in the daily practice even more.

In this study, we compare the geometrically non-linear structural response of a 34 m wind turbine blade under flap-wise loading with a linear response. Focus was on the evaluation of the mean and design resistance in the ultimate strength and stability limit states. We analysed the design resistance according to the least stringent GL requirements and compared the results with non-linear approaches proposed by GL and Eurocode, which require the application of an imperfection. Also, we applied imperfections according to Eurocode, which appeared more realistic compared with GL's approach.

This study is structured as follows: the second section introduces the normative analysis requirements and terms in limit state design (LSD) used in standards needed to understand the conducted evaluations in this work. In Section 3, we describe the numerical computation methodology. Further, we explain how the material safety factors are applied for different analysis types. In Section 4, we present the results of the validations according to GL and Eurocode and describe the influence of imperfections. In Section 5, we discuss the results of the numerical computations in comparison with a full-scale test and propose future investigations. Finally, we present the main conclusions in Section 6.

The LA revealed an unrealistic failure mechanism and failure mode. Further, it did not capture the highly non-linear response of the blade that was measured in an ultimate full-scale test to failure and determined by a GNA. More realistic non-linear approaches proposed by GL and Eurocode yielded more optimistic results than the mandatory linear bifurcation analysis (LBA). Consequently, the investigated blade designed after the least stringent requirements was sufficient. Using the non-linear approaches, considering inter-fibre failure (IFF) as the critical failure mode, yielded still a significant safety margin for the designer (7–28%). The non-linear response was significantly dependent on the scaling of the applied imperfection.

2. NORMATIVE ANALYSIS REQUIREMENTS

Since the focus of this study is to investigate the response of the blade due to analyses according to GL, we briefly introduce the safety factors used in LSD, also called load and resistance factor design. GL guideline and Eurocode are based on LSD, which is defined in ISO 2394.¹⁶ Further, we show how we distinguish between analysis methods in this study and present excerpts of GL's and Eurocode's analysis methods.

2.1. Ultimate limit state function

Referring to ISO 2394,¹⁶ an ultimate limit state g is defined as function of basic variables, which characterize the design values: (i) actions and environmental influences F_d , (ii) properties of materials f_d and (iii) geometrical parameters a_d :

$$g(F_d, f_d, a_d, \gamma_n) \geq 0 \quad (1)$$

Further, the coefficient γ_n takes the importance of the structure and the consequence of failure into account.

2.2. Partial factors

In the standards and guidelines used in wind energy, the partial factors format is usually applied to determine the design values.

The partial safety factor for the internal loads γ_f accounts for possible unfavourable load deviations and uncertainties in the loading model according to IEC 61400-1:¹⁷ it is distinguished between normal ($\gamma_f = 1.35$) and abnormal design

load cases ($\gamma_f = 1.1$). Multiplying γ_f by the characteristic load value F_k , derived from aero-elastic simulations, yields the design value F_d :

$$F_d = \gamma_f F_k \quad (2)$$

The partial safety factor for materials γ_m accounts for unfavourable deviations of the strength and possible inaccurate assessment of the resistance of sections or load-carrying capacity of parts of the structure. Also accounted for are uncertainties (i) in the geometrical parameters, (ii) in the relation between the material properties in the structure and those measured in tests on control specimens and (iii) in conversion factors.¹⁷ Dividing characteristic material properties f_k —such as material strengths or moduli by γ_m —yields the design property f_d :

$$f_d = \frac{f_k}{\gamma_m} \quad (3)$$

where the characteristic material properties f_k are derived from measurements assuming a 95% confidence level of a normal distribution as proposed GL.¹³

The design value of geometrical quantities a_d is determined from the characteristic geometry a_k and additive geometrical quantities Δa , such as geometric imperfections:

$$a_d = a_k \pm \Delta a \quad (4)$$

The partial safety factor for the consequence of failure γ_n depends on the component class. Rotor blades fall under class 2 ($\gamma_n = 1.0$) representing a ‘non fail-safe’ structural component, which failure may lead to the failure of a major part.¹⁷

For the design validation, a full-scale blade test is conducted according to IEC 61400-23.¹⁸ The partial safety factor $\gamma_s = 1.1$ is defined, which accounts for the blade-to-blade variation of a series. Further, the factor γ_l is defined accounting for the environmental conditions at the test site. Both factors plus γ_n are applied on the design load F_d to reveal the target loading F_{target} :

$$F_{\text{target}} = F_d \gamma_n \gamma_s \gamma_l \quad (5)$$

2.3. Load effect and resistance

The design values of the limit state function (equation (1)) can be separated into two groups. The first group covers the load or action effects S_d :

$$S_d = S(F_d, f_d, a_d) \quad (6)$$

The load effect can be a function of f_d when the stiffness—such as Young’s and shear modulus—is considered as design values, i.e. in a buckling analysis. The second group covers the resistances:

$$R_d = R(F_d, f_d) \quad (7)$$

The resistance can be a function of F_d when the material properties are dependent of the load, i.e. in a material non-LA. A design is evaluated successfully when the design criterion is fulfilled, that is the load effect (equation (6)) yields a lower or lower or equal value than the resistance (equation (7)):

$$\gamma_n S_d \leq R_d \quad (8)$$

In case of the evaluation of fibre-reinforced plastics, mostly failure criteria or indices FI are used, e.g. Tsai/Wu¹⁹ or Puck.²⁰ These criteria are defined as function of load effect and resistance:

$$FI(\gamma_n S_d, R_d) \leq 1 \quad (9)$$

We define two indicators for the ‘load carrying capacity’ of a structure: (i) safety reserve factor and (ii) margin of safety. The safety reserve factor is defined as ratio between the design resistance and the design load effect:

$$\text{Safety Reserve Factor (SRF)} = \frac{R_d}{S_d} \quad (10)$$

Considering the load history of the external load P , its value at the design point is defined as P_d . Further, the external load at failure is considered as P_f . In other words, the external load at failure is reached, when the design load effect is equal to the design resistance ($S_d = R_d$); or $FI = 1$. Hence, the margin of safety is defined as follows:

$$\text{Margin of Safety (MoS)} = \frac{P_f}{P_d} - 1 \quad (11)$$

2.4. Numerical analysis concepts

Referring to Eurocode,¹⁵ we used the following abbreviations for analysis concepts in this study:

- LA = linear analysis
- LBA = linear bifurcation analysis
- GNA = geometrically non-linear analysis
- GNIA = geometrically non-linear analysis with imperfections
- GN(I)A + LBA = geometrically non-linear analysis (with imperfections) combined with an LBA during the load path

2.5. Execution according to GL guideline

The ultimate strength and stability limit state analyses are mandatorily conducted as linear static analysis (LA) and as LBA, respectively. Referring to VDI 2014,²¹ the Tsai/Wu failure criterion can be used as failure index if it is modified to obtain IFF and fibre failure (FF) according to the Puck/Knaust criterion.²² This procedure is shown in the Appendix.

Also, the stability limit state analysis can be conducted in terms of a geometrically non-linear strength analysis with imperfections (GNIA). Therefore, the following GL recommendations are considered:¹³

- A pre-deformation affine to the first critical linear buckling eigenmode due to an LBA is applied globally to the perfect model.
- The whole mode shape is scaled so that the buckle height Δw_0 of the eigenmode's most critical buckle is derived by the product of its largest horizontal dimension (diameter l_g as shown in Figure 3(b)) and a dimple tolerance factor $U_0 = 1/400$:

$$\Delta w_0 = l_g U_0 \quad (12)$$

A smaller pre-deformation is permitted if the buckle height Δw_0 is verified.

- This pre-deformed model has to undergo an FF analysis.
- A material safety factor $C_{1a} = 1.35$ for the influence of ageing has to be applied on the material strength.
- The partial material safety factor for stability γ_{mc} is applied either on the stresses (variant A in this study) or on the material stiffnesses (variant B in this study).
- Additionally, an LBA is required to verify that the buckling resistance* of the first eigenmode is larger than the strength resistance.

2.6. Execution according to Eurocode

In general, GL's analysis concepts described previously are the most conservative excerpts of Eurocode's possible analysis methods for shell structures made from steel.

In addition to the analysis concepts used in GL, Eurocode¹⁵ states that the ultimate stability limit state may also be evaluated by a geometrically non-linear strength analysis with imperfections combined with an LBA during the load path (GNIA + LBA). Here, the total load to be applied on the structure is split into load increments. After each increment, the buckling resistance is determined by an LBA. The smallest resistance—either due to a strength analysis using a GNIA or due to the LBA conducted during GNIA's load path—is relevant for the evaluation.

Additional to GL's method to apply a geometric imperfection, Eurocode states that imperfections may be excluded when they are unrealistic because of manufacturing or erecting. That is, instead of the global pre-deformation of the whole first eigenmode, a simple dimple can be modelled as imperfection. The dimple amplitude Δw_0 is derived with equation (12), where l_g is the relevant length of the dimple. However, the used pre-deformation represents always the 'worst' imperfection.

3. METHODS

3.1. Finite element model

In our numerical investigations, *MSC PATRAN* 2013 was used as pre-processor and post-processor, and *MSC Marc* 2010 was applied as solver for all analyses. The FE model consisted of 83,684 elements and 575,479 nodes. Its structure was represented by a 20 node hexahedron continuum composite brick element (element 150 in *Marc* library²³). Using solid elements in blade design is permissible according to GL.¹³

*Sometimes the 'buckling resistance' is called 'buckling load'. To have a consistent differentiation between load effect and resistance in the sense of LSD, the load at which the structure is unstable is considered as 'buckling resistance' in this paper.

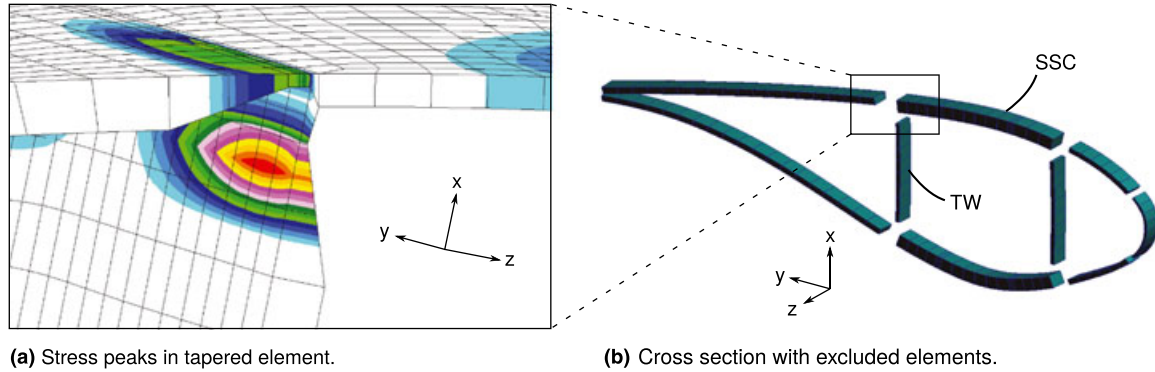


Figure 1. Exclusion of tapered elements. The suction side cap (SSC) and the trailing web (TW) are critical structures: (a) stress peaks in tapered element and (b) cross section with excluded elements.

In Rosemeier,²⁴ the FE model was verified with analytical models and validated with a full-scale static certification test²⁵ and further full-scale tests conducted at DTU Wind Energy. The global deflection of the blade, the local out-of-plane displacement of the cap and the longitudinal strain were in good agreement with the tests.

One weakness using a three-dimensional (3D) composite brick element is that tapered sandwich structures²⁶ are not properly modelled. This means that within these elements, the plies of the facings loose their stiffness erroneously because the thickness is reduced by the tapering.²⁴ The loss of flexibility leads to high stress peaks as shown in Figure 1(a). Since we do not expect failure in these elements, we excluded them as shown in Figure 1(b).

3.2. Materials

The blade design of the considered 34 m blade consisted of a load-carrying box girder covered by two aerodynamic shells glued to the box. The box girders cap's layup mainly consisted of glass fibre-reinforced uniaxial and biaxial material, and the girder's webs consisted of a biaxial layup covering a core material. The panels of the aerodynamic shell consisted of sandwich layups. Since only two-dimensional material data were available, the 3D linear material model was modified by adjusting the Poisson's ratios to meet shell-like (two-dimensional) material behaviour. A linear material model was used in the FE analysis because GL does not require non-linear material modelling.

3.3. Load application

The load case applied to the FE model was derived from the load distribution of the full-scale certification test F_{test} (Figure 2). According to the test,⁵ we applied point forces at five positions on the blade span in flap-wise direction so that the suction side cap was under compression. Further, the positions of load introduction were chosen not to constrain critical structural areas. To distribute the forces on the caps, we used a linear interpolation element (RBE3 *Marc* library²⁷), which does not constrain the cross sections.

To make our investigations comparable with test, the test load F_{test} was assumed to be equal to the target load F_{target} to derive the design load F_d using equation (5). Comparing the test and target load distributions in Figure 2, this assumption leads to an overloading. Thus, the assumed design load in this study was slightly more conservative over some parts of the blade than the design load used for the real design of the considered blade. Referring to Jensen *et al.*,⁵ the partial safety factor for the environmental influences at the test site was set to $\gamma_1 = 1.0$. The full-scale test to failure was conducted after the static and fatigue certification tests.

To derive the characteristic load F_k using equation (2), we assumed that the load envelope consisted of abnormal design load cases ($\gamma_f = 1.1$); the blade was certified for the wind turbine-type class II.²⁸

3.4. Numerical analyses concepts

3.4.1. Linear bifurcation analysis.

The LBA is formulated as eigenvalue problem:

$$(\mathbf{K} - \lambda \mathbf{K}_G) \Phi = \mathbf{0} \quad (13)$$

where \mathbf{K} is the stiffness matrix, \mathbf{K}_G is the geometric stiffness matrix (or stress stiffness matrix), λ is the n th eigenvalue and Φ is the displacement eigenvector of the n th eigenvalue. The solution of the eigenvalue problem (equation (13)) reveals n eigenvalues, which are used to obtain the corresponding n linear buckling resistances P_{cr} with respect to its buckling modes:

$$P_{cr} = \lambda P \quad (14)$$

3.4.2. Geometrically non-linear analysis.

The following properties were set in *MSC Marc* for the geometrically non-linear static simulations (GN(I)A):

- The applied forces followed the structural deformation (FOLLOW FOR).
- Large strains were regarded for the solution of equilibrium equations (LARGE STRAIN).
- Large displacements were regarded for the solution of equilibrium equations (LARGE DISP).

3.4.3. Geometrically non-linear analysis with linear bifurcation analysis during the load path.

The GN(I)A + LBA concept is a combination of the two aforementioned analyses. In *MSC Marc*,²⁹ this concept is called non-linear buckling analysis and is expressed as the eigenvalue problem in equation (13). The geometric stiffness matrix \mathbf{K}_G , however, is assumed to be a linear function of the load increment ΔP and is based on the stress $\Delta\sigma$ and displacement state change $\Delta\mathbf{u}$ compared with the beginning of the last increment:

$$(\mathbf{K} - \lambda \Delta\mathbf{K}_G(\Delta\mathbf{u}, \mathbf{u}, \Delta\sigma)) \Phi = \mathbf{0} \quad (15)$$

The stress and strain states are not updated during the bifurcation analysis. Thus, for the n th buckling mode, the buckling resistance $P_{cr,i}$ of each external load step i is estimated by

$$P_{cr,i} = P_{i-1} + \lambda_i \Delta P \quad (16)$$

where P_{i-1} is the external load level—prior to the load increment by which the LBA is conducted. λ_i is obtained by the eigenvalue problem solved at each load step i using the power sweep or Lanczos method.

3.5. Strength analysis

This section is divided into two parts presenting the evaluation method using (i) mean material strength f_m and (ii) design material strength f_d (equation (3)) as resistance (equation (7)). As failure index, a modified Tsai/Wu criterion was

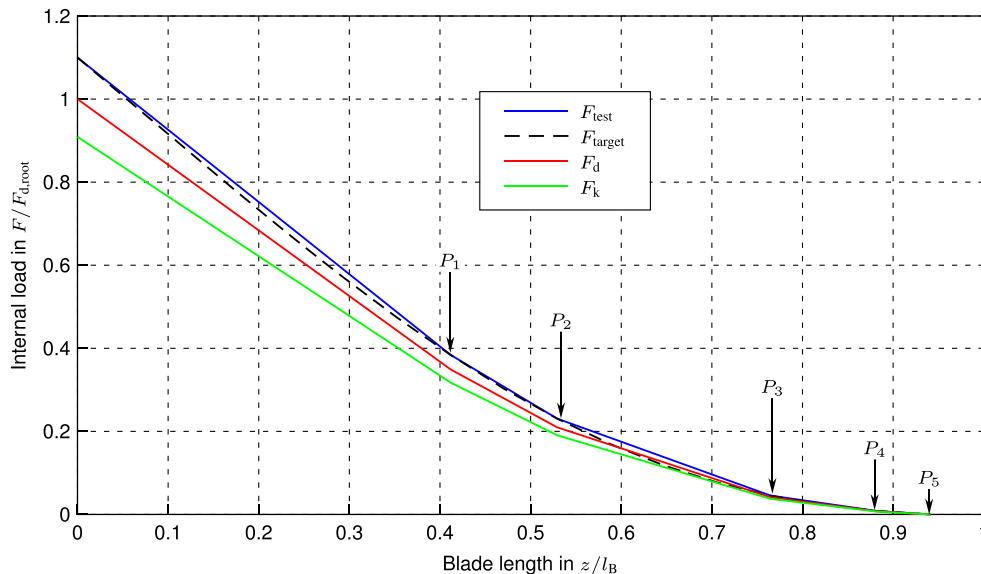


Figure 2. Load distributions applied in the full-scale test F_{test} and in the numerical model (F_d and F_k). The vectors P indicate the positions of the external point forces applied in the test and in the numerical model.

used to identify IFF and FF. The safety factor for the consequence of failure γ_n is always set equal to 1.0 according to IEC.¹⁷

The strength analysis was performed as GNA and LA. For the GNA, a report of all elements excluding the tapered elements—as explained previously—was post-processed at the load level before instability of the model. These reported results were searched for the most critical locations and its layers. Afterwards, the failure indices for the whole load history were plotted. This process was performed for the LA as well. After deriving the load history, we calculated the safety reserve factor (*SRF*) and the margin of safety (*MoS*) for the mean and design resistance.

3.5.1. Mean resistance.

We investigated the mean strength resistance for IFF to show the linear and non-linear structural response without application of safety factors. An evaluation using mean values is not required in a certification. Because the difference between design and mean resistance, however, is large, we choose this way to illustrate the effect of non-linearities without safety factors.

Considering equation (9) and multiplying the load effect S_d by $\gamma_n = 1.0$, the failure index is expressed as follows:

$$FI_{m,IFF}(S_d(F_d), R_m(f_{m,strengths})) \leq 1 \tag{17}$$

where F_d is the design load. The mean resistance is expressed as function of the mean material strengths:

$$R_m(f_{m,strengths}) = R_m(R_{\parallel}^t, R_{\parallel}^c, R_{\perp}^t, R_{\perp}^c, R_{\perp\parallel}, R_{\perp\perp}) \tag{18}$$

where the indices t and c stand for, respectively, tension and compression, and the indices \parallel and \perp stand for, respectively, parallel and perpendicular to the fibre axis orientation. According to VDI 2014,²¹ the strengths in fibre direction are increased for IFF. We chose the mean factor of 1.4 (range 1.3...1.5) so that $R_{\parallel,IFF} = 1.4 R_{\parallel}$. To obtain IFF according to Puck/Knaust, the coefficients F_{11}, F_1, F_{44} and F_{23} need to be modified in the Tsai/Wu failure criterion (Appendix). Thus, the transverse/transverse shear strength is calculated by

$$R_{\perp\perp} = \sqrt{\frac{1}{3} R_{\perp}^t R_{\perp}^c} \tag{19}$$

At design load level, the load-carrying capacity in terms of the safety reserve factor *SRF* is calculated using equation (10):

$$SRF = \frac{R_m}{S_d} = \frac{1}{FI_{m,IFF}} \tag{20}$$

where F_d represents the internal load as function of the external load level P_d . Deriving the load at failure P_f , at which $FI_{m,IFF} = 1$ (compare Figure 4), we calculated the load-carrying capacity in terms of the margin of safety *MoS* (equation (11)).

3.5.2. GL design resistance.

We investigated the design resistance to show whether the evaluation is successful when the safety factors are applied according to GL guideline. The GL guideline distinguishes between load effect and resistance being considered for FF and IFF. In the FF analysis, the partial safety factor for the loads γ_f is applied on the characteristic load F_k (equation (2)) and the partial safety factor for materials $\gamma_{m,FF}$ on the characteristic material properties f_k (equation (3)). In the IFF analysis, the characteristic load F_k is used without safety factors, and $\gamma_{m,IFF}$ is applied on the mean material strengths f_m . To derive the design material strength for the FF and IFF analysis, the characteristic f_k and mean f_m strengths are reduced, respectively.

The partial material safety factor for FF strength used in this study is the product of GL:¹³ the general material safety $\gamma_{m0} = 1.35$, the influence of ageing $C_{1a} = 1.35$, the temperature effect $C_{2a} = 1.1$, the manufacturing process $C_{3a} = 1.1$ and the effect of post-curing $C_{4a} = 1.0$. To identify FF, the Tsai/Wu criterion is modified:²¹ the strengths in non-fibre directions ($R_{\perp}^t, R_{\perp}^c, R_{\perp\parallel}$ and $R_{\perp\perp}$) are increased to unrealistically high values (10^4N mm^{-2}). The evaluation of FF in terms of the failure index (equation (9)) is expressed as follows:

$$FI_{d,FF} \left(S_d \left(\underbrace{\gamma_f}_{1.1} F_k \right), R_d \left(\frac{f_{k,strengths}}{\underbrace{\gamma_{m0} C_{1a} C_{2a} C_{3a} C_{4a}}_{\gamma_{ma,FF}=2.21}} \right) \right) \leq 1 \tag{21}$$

The partial material safety factor for IFF strength used in this study is the product of GL:¹³ the general material safety $\gamma_{m0} = 1.35$ and $C_{\text{IFF}} = 1.25$ (accounts for changes of material properties due to temperature, ageing, etc.). The failure index for the evaluation of IFF is then expressed as follows:

$$FI_{d,\text{IFF}} \left(S_d(F_k), R_d \left(\frac{f_{m,\text{strengths}}}{\underbrace{\gamma_{m0} C_{\text{IFF}}}_{\gamma_{\text{ma,IFF}}=1.69}} \right) \right) \leq 1 \quad (22)$$

The *SRF* and *MoS* are then calculated in the sense of equations (20) and (11) as explained previously.

3.6. Stability analysis

The mean stability analysis was performed by (i) an LBA and (ii) a GNA with bifurcation analysis during the load path (GNA + LBA).

Further, the design stability resistance was determined by four different analyses: the first two are both variants of the non-linear stability analysis according to GL guideline as explained in Section 2.5: (i) variant A, where the material safety factors are applied on the internal load, and (ii) variant B, where the material safety factors are applied on Young's and shear moduli of the materials. Both variants use a GNA. Moreover, the third and fourth analysis methods used were as follows: (iii) an LBA with safety factors and (iv) a GNA + LBA.

3.6.1. Mean resistance.

Linear bifurcation analysis. An LBA—using Lanczos method—revealed the first five eigenmodes and eigenvectors. The design criterion (equation (8)) is expressed as follows:

$$\underbrace{S_d(F_d, f_m)}_{P_d} \leq \underbrace{R_m}_{P_{\text{cr,m}}} \quad (23)$$

To determine the *SRF* (equation (10)), the external design load P_d is considered as load effect and the critical buckling resistance $P_{\text{cr,m}}$ as resistance. Considering the buckling resistance $P_{\text{cr,m}}$ as load where the structure fails P_f , the *MoS* is calculated using equation (11).

Geometrically non-linear bifurcation analysis. The total applied load of $2P_{\text{Test}}$ was divided into 20 load increments. The Lanczos method was used for the first 10 increments and the inverse power sweep method for increments 11–15. Since the inverse power sweep method yielded unusable results as the load was close to the buckling resistance, we extrapolated the last increments of the critical mode shapes' curves (GNA + LBA at 8.3% and 32.3% l_B in Figure 6) to obtain the critical buckling resistance at failure P_f . The *SRF* and *MoS* are then calculated using equations (10) and (11), respectively.

3.6.2. Design resistance.

Four different methods were used to evaluate the design stability resistance. This time, the safety factors were applied on the material properties of the model. Furthermore, an initial imperfection was applied for three of the aforementioned analyses to the model: (i) variant A, (ii) variant B and (iii) geometrically non-LBA. Thus, the application of the imperfection according to GL guideline is explained first. Then, the following sections describe the four conducted analyses in detail.

Imperfection. The initial imperfection is applied according to GL. It is represented by the first critical buckling mode shape gained by an LBA in the following procedure:

1. Determine the most critical dimple of the buckling mode shape (Figure 3(a)).
2. Obtain its largest horizontal dimension l_g (Figure 3(b)).
3. Create a vector field of the whole deformation according to the mode shape as shown in Figure 3(a).
4. Scale the vector field so that the height of the critical dimple is $\Delta w_0 = U_0 l_g$, where $U_0 = 1/400$ is GL's dimple tolerance factor (Figure 3(c)).
5. Apply the scaled deformation to the model.

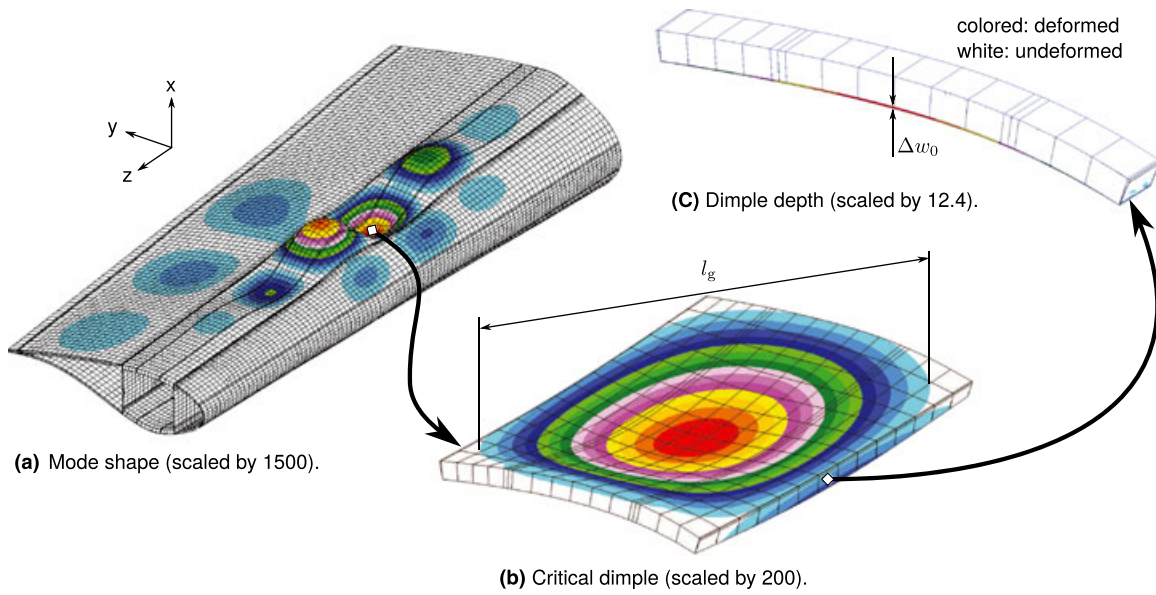


Figure 3. Application of the imperfection: (a) mode shape (scaled by 1500), (b) critical dimple (scaled by 200) and (c) dimple depth (scaled by 12.4).

In our model, this procedure revealed an inward initial dimple depth of the following equation (Figure 3(c) illustrates the quantitative effect):

$$\Delta w_0 = l_g U_0 = 0.9 \text{ m} \cdot 1/400 = 2.250 \text{ mm} \quad (24)$$

GL variant A. According to GL, the stability resistance is evaluated by a geometrically non-linear strength analysis with imperfections (GNIA), where FF is mandatorily considered for the evaluation. IFF, however, was also analysed to show the structural response compared with FF. The partial material safety factor for stability γ_{mc} is the product of GL:¹³ the general material safety $\gamma_{m0} = 1.35$, the scattering of the moduli $C_{1c} = 1.1$ and the temperature effect $C_{2c} = 1.1$. γ_{mc} is applied on the stresses. Further factors are applied on stresses: for the FF analysis, the partial material safety factor for strength C_{1a} (influence of ageing), and for the IFF analysis, the safety factor for strength C_{IFF} (accounts for changes of material properties due to temperature, ageing, etc.). The design stability resistance is evaluated using the modified Tsai/Wu criterion as failure index as described in Section 3.5.2. Using the Tsai/Wu criterion, we could divide the strengths ($R_{\parallel}^t, R_{\parallel}^c, R_{\perp}^t, R_{\perp}^c, R_{\perp\parallel}, R_{\perp\perp}$) by γ_{mc} rather than multiplying γ_{mc} by the stresses σ_i and τ_{ij} (see expression of Tsai/Wu criterion in the Appendix). This strategy is useful in *MSC Patran*, which provides only an interface to the strengths of a failure index.

Considering equation (4), a_k represents the perfect model and Δa the applied imperfection as function of U_0 . The design value of geometrical quantities a_d is counted to the group of load effects S_d . Thus, the design criterion for FF is expressed as follows:

$$FI_{d,FF} \left(S_d \left(\underbrace{\gamma_f}_{1.1} F_k, \underbrace{a_{d,imperfection}}_{U_0=1/400} \right), R_d \left(\frac{f_{k,strengths}}{\underbrace{\gamma_{m0} C_{1c} C_{2c}}_{\gamma_{mc}=1.63} \underbrace{C_{1a}}_{1.35}} \right) \right) \leq 1 \quad (25)$$

and for IFF as

$$FI_{d,IFF} \left(S_d \left(F_k, \underbrace{a_{d,imperfection}}_{U_0=1/400} \right), R_d \left(\frac{f_{m,strengths}}{\underbrace{\gamma_{m0} C_{1c} C_{2c}}_{\gamma_{mc}=1.63} \underbrace{C_{IFF}}_{1.25}} \right) \right) \leq 1 \quad (26)$$

GL variant B. The different methodology to variant A is that the material safety factor for stability is applied on the moduli. Thus, the design criterion for FF is expressed as follows:

$$FI_{d,FF} \left(S_d \left(\underbrace{\gamma_f}_{1.1} F_k, \underbrace{\frac{f_{m,moduli}}{\gamma_{m0} C_{1c} C_{2c}}}_{\gamma_{mc}=1.63}, \underbrace{a_{d,imperfect}}_{U_0=1/400} \right), R_d \left(\underbrace{\frac{f_{k,strengths}}{C_{1a}}}_{1.35} \right) \right) \leq 1 \quad (27)$$

and for IFF as

$$FI_{d,IFF} \left(S_d \left(F_k, \underbrace{\frac{f_{m,moduli}}{\gamma_{m0} C_{1c} C_{2c}}}_{\gamma_{mc}=1.63}, \underbrace{a_{d,imperfect}}_{U_0=1/400} \right), R_d \left(\underbrace{\frac{f_{m,strengths}}{C_{IFF}}}_{1.25} \right) \right) \leq 1 \quad (28)$$

GL linear bifurcation analysis. According to GL, an LBA is mandatory to evaluate the buckling resistance $P_{cr,d}$. The LBA is conducted without an imperfection. For the evaluation, the moduli are reduced by γ_{mc} including the safety factor C_{3c} (inaccuracy between linear and non-LA). Thus, the design criterion (equation (23)) can be extended to

$$S_d \left(\underbrace{\underbrace{\gamma_f}_{1.1} F_k, \underbrace{\frac{f_{m,moduli}}{\gamma_{m0} C_{1c} C_{2c} C_{3c}}}_{\gamma_{mc}=2.04}}_{P_d} \right) \leq \underbrace{R_d}_{P_{cr,d}} \quad (29)$$

Eurocode geometrically non-linear bifurcation analysis. To compare the three GL approaches shown in the previous paragraphs, we also conducted one of the Eurocode's evaluation methods: a GNIA + LBA. In general, this analysis method has the same manner as the GNA + LBA, described in Section 3.6.1, plus the application of the imperfection. In comparison with GL's LBA, the factor C_{3c} is excluded because inaccuracy due to an LA cannot occur. Lanczos method was used with 20 increments. We extrapolated the last increments. Thus, the design criterion (equation (29)) can be modified to

$$S_d \left(\underbrace{\gamma_f}_{1.1} F_k, \underbrace{\frac{f_{m,moduli}}{\gamma_{m0} C_{1c} C_{2c}}}_{\gamma_{mc}=1.63}, \underbrace{a_{d,imperfect}}_{U_0=1/400} \right) \leq R_d \quad (30)$$

3.7. Introduction of imperfections

To investigate the influence of the imperfections, we pre-deformed the model in two ways: (i) by global scaling of the whole mode shape as shown in Figure 3(a) and (ii) by local modification regarding merely the critical buckle of the mode shape as shown in Figure 3(b).

Global scaling. We scaled the mode shape at 32.3% blade length (Figure 7) globally with three different dimple tolerance factors, $U_0 = 1/200, 1/400, 1/800$ (equation (12)), where the relevant length of the dimple of our model was $l_g = 0.9$ m. The pre-deformation was applied as described in GL guideline (Section 3.6.2). Afterwards, a GNIA without any safety factors as described for the mean strength resistance in Section 3.5.1 was performed. The Tsai/Wu criterion (non-modified) was used to analyse the structural response. To compare the relative influence between different imperfection scalings, the load at failure of the blade with imperfection $P_{f,imperfect}$ is divided by the load at failure of the blade without an imperfection $P_{f,perfect}$.

Local modification. According to Eurocode, imperfections can be excluded from the pre-deformation when they are unrealistic because of the manufacturing process. Thus, we merely modified the critical buckle of the mode shape locally, considering the maximum initial dimple as shown in Figure 3(b). Again, the pre-deformation was applied as described in GL guideline (Section 3.6.2), but the vector field was merely created for the maximum initial dimple. The dimple tolerance factor was $U_0 = 1/400$ (equation (12)), where the relevant length of the dimple of our model was $l_g = 0.9$ m. Then, we applied the dimple in two simulations inwards and outwards, respectively. The vector field of the outwards dimple was the inverted vector field of the inwards dimple.

4. RESULTS

4.1. Strength analysis

4.1.1. Mean resistance.

We investigated the mean strength resistance to show the linear (LA) and non-linear (GNA) structural response without application of safety factors. The results of a GNA and an LA simulation for the first three critical locations (Figure 5(a)) are compared as shown in Figure 4. The curves of LA show a parabolic shape due to the quadratic terms in the Tsai/Wu criterion.¹⁹ In contrast, the curves of GNA show a more non-linear behaviour, which indicates a structural response due to buckling. After evaluation of the design criterion (equation (17)), we determined the safety reserve using equations (20) and (11) (Table I). In general, we found that the GNA was more conservative than the LA. Moreover, the critical failure location and mechanism of both calculation methods were different. By investigation via GNA, the most critical location on the blade at design load P_d (at 25.1% blade length l_B) is different from the critical location at load at failure $1.8 P_d$ (at 8.3% l_B shown in Figure 5(b)).

4.1.2. GL design resistance.

The evaluation of the design strength resistance—including the GL safety factors for FF (equation (21)) and IFF (equation (22))—was successful (Table II). As found for the IFF evaluation of the mean resistance, the GNA was more conservative than the LA. Comparing the *MoS* for FF strength, the GNA was also more conservative than LA. Comparing the *SRF* for FF strength at 34.0% l_B , however, shows that GNA and LA were quite close. Considering only LA, FF is more critical than IFF.

4.2. Stability analysis

4.2.1. Mean resistance.

A GNIA + LBA reveals three buckling modes at 8.3%, 32.3% and 66.7% of the blade length l_B . For two modes (8.3% and 32.3% l_B), the buckling resistance P_{CR} decreases over the load history, whereas for the third mode (66.7% l_B), the resistance increases (Figure 6). The two ‘decreasing’ mode shapes had its critical buckle on the suction side cap, whereas

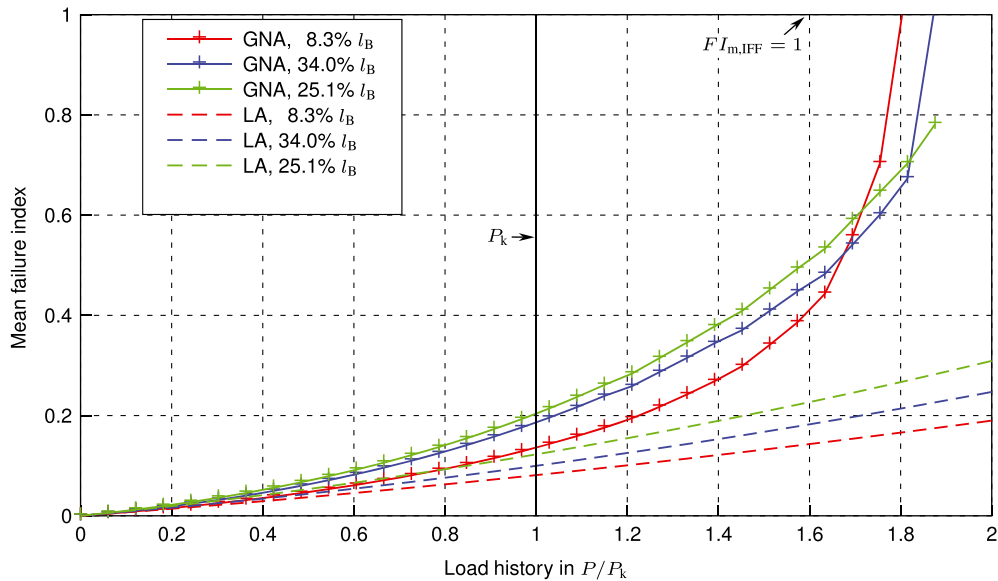


Figure 4. Mean strength resistance.

Table I. Evaluation of the mean strength.

Method	<i>MoS</i> (%)	<i>SRF</i>	z/l_B (%)	Failure mode	Failing layer
LA	431.5	8.2	25.1	IFF	Suction side cap (SSC), first inner uniaxial layer
GNA	80.3	7.3	8.3	IFF	Suction side cap (SSC), first inner uniaxial layer
GNA	104.4	4.9	25.1	IFF	Suction side cap (SSC), first inner uniaxial layer

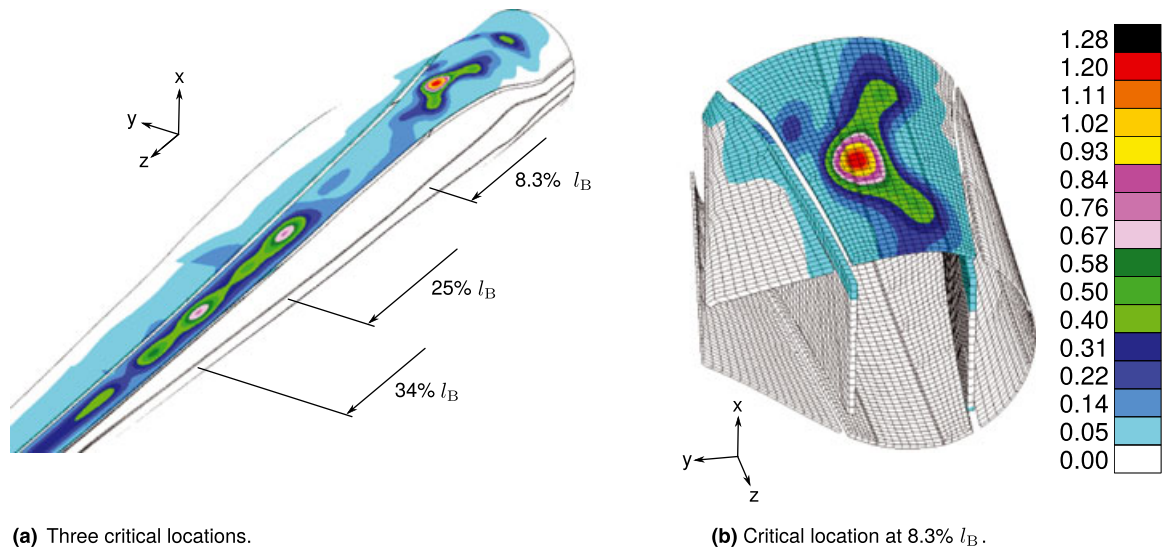


Figure 5. Critical locations at $1.8 P_d$ due to the GNA. The colour scale shows the modified Tsai/Wu failure index for inter-fibre failure: (a) three critical locations and (b) critical location at $8.3\% l_B$.

Table II. Evaluation of the design strength.

Method	MoS (%)	SRF	z/l_B (%)	Failure mode	Failing layer
LA	154.0	4.0	25.7	IFF	Suction side cap (SSC), first inner uniaxial layer
GNA	55.1	2.5	25.1	IFF	Suction side cap (SSC), first inner uniaxial layer
LA	122.7	3.7	34.0	FF	Suction side cap (SSC), first inner uniaxial layer
GNA	73.1	3.9	34.0	FF	Suction side cap (SSC), first inner uniaxial layer

Table III. Evaluation of mean buckling resistance due to bifurcation analysis.

Method	MoS (%)	SRF	z/l_B (%)	Failure element
LBA	89.1	1.89	32.3	Suction side cap (SSC)
GNA + LBA	76.0	1.87	32.3	Suction side cap (SSC)
GNA + LBA	68.7	1.96	8.3	Suction side cap (SSC)

the third ‘increasing’ mode shape had its highest buckle on the suction side trailing shell (Figure 7). At design load P_d , the mode at $32.3\% l_B$ is the most critical. This mode is different from the critical mode at failure ($P = P_{cr}$); here, it is the mode at $8.3\% l_B$. Notice that we extrapolated the curves for 8.3% and $32.2\% l_B$ for the last increments (dashed lines in Figure 6) up to the point of instability. Comparing the buckling resistance of GNA + LBA with the LBA, we found that GNA + LBA yields the lower result (Table III). Moreover, the failure load of the mean strength analysis (Figure 4) is reached before the buckling resistance due to either GNIA + LBA or LBA. The investigated evaluation is expressed in equation (23).

4.2.2. GL design resistance according to the geometrically non-linear analysis with imperfections.

According to GL, it is possible to apply the material safety factor either on the stresses or on the material moduli. The difference of these two variants is investigated in the following. Moreover, the stability analysis can be conducted as geometrically non-linear strength analysis with imperfections (GNIA). We used the modified Tsai/Wu criterion as failure index for the evaluation of the FF and IFF design stability resistance.

The results of a GNIA show that the application of an imperfection has a significant influence on the strength resistance at that location where we applied the imperfection ($32.3\% l_B$). The failure index for variant A is expressed in equations (25) and (26). Here, the safety factor reduces the allowable strengths, which is equivalent to the increase of the stresses (Section 3.6.2). The failure index for variant B is expressed in equations (27) and (28). Here, the safety factor is applied on the moduli. Variant B shows a flatter slope than A at low load level turning into a higher slope than

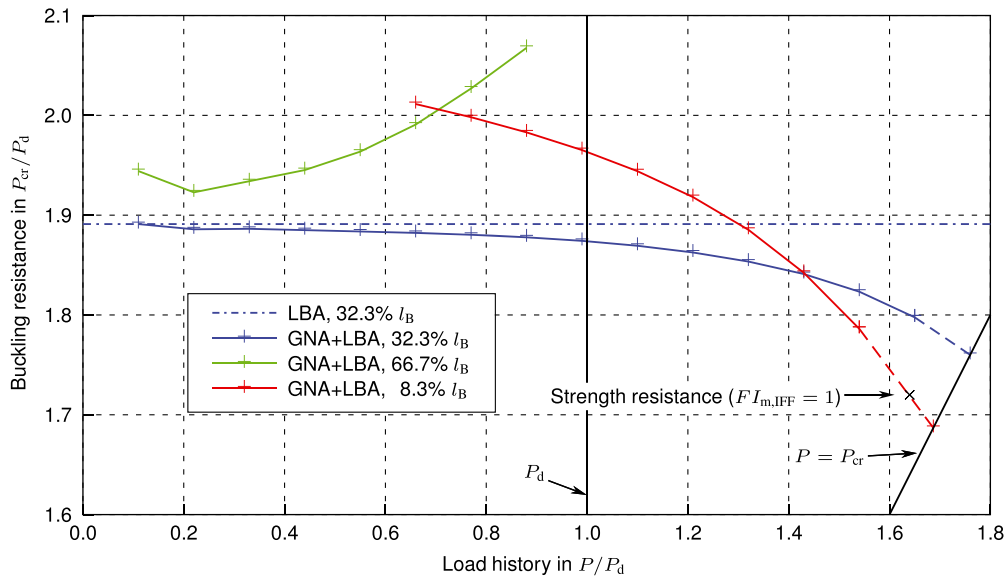


Figure 6. Mean buckling resistance. The last increments of the curves GNA + LBA at 8.3% and 32.3% l_B are extrapolated. In addition, the critical point according to the strength analysis—where the mean failure index $F_{I_{m,IFF}} = 1$ —is marked.

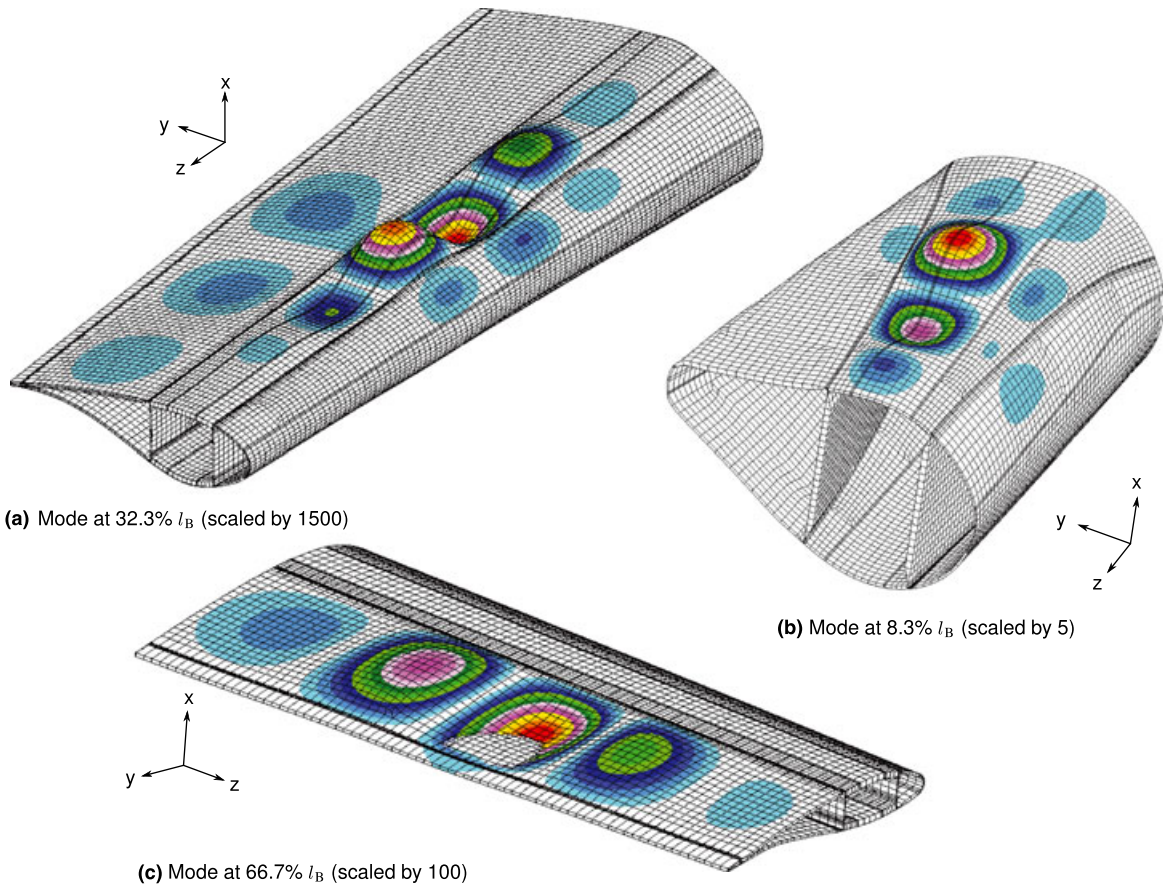


Figure 7. Buckling mode shapes: (a) mode at 32.3% l_B (scaled by 1500), (b) mode at 8.3% l_B (scaled by 5) and (c) mode at 66.7% l_B (scaled by 100).

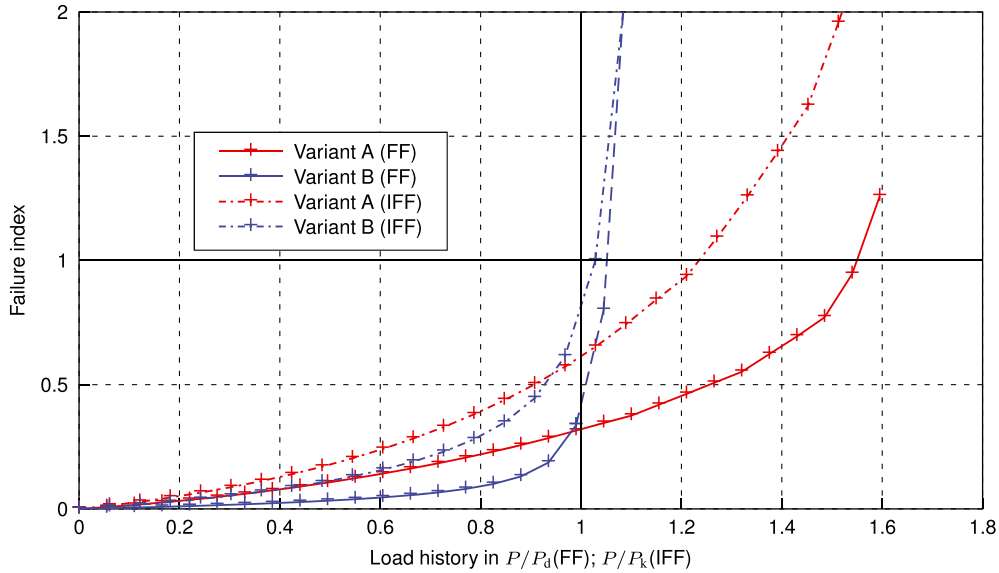


Figure 8. Design buckling resistance (variants A and B).

Table IV. Evaluation of design buckling resistance due to variants A and B.

Method	MoS (%)	z/l_B (%)	Failure mode	Failing layer
GNIA (variant A)	55.0	34.0	FF	Suction side cap (SSC), first inner uniaxial layer
GNIA (variant B)	5.1	34.0	FF	Suction side cap (SSC), first inner biaxial layer (-45°)
GNIA (variant A)	23.5	35.6	IFF	Suction side cap (SSC), first inner uniaxial layer
GNIA (variant B)	2.9	30.9	IFF	Suction side cap (SSC), first inner uniaxial layer

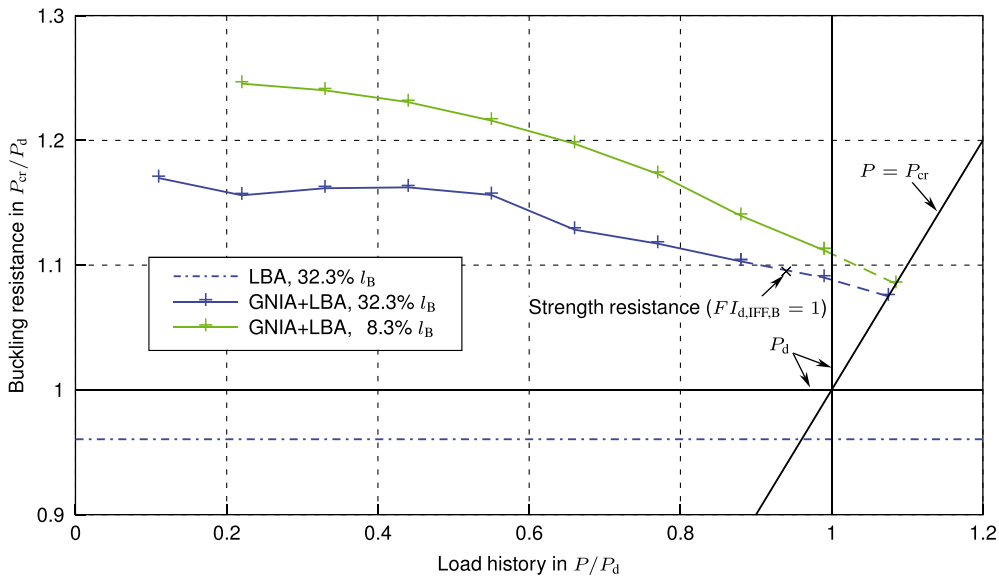


Figure 9. Design buckling resistance (bifurcation analysis). The last increments of the curves GNA + LBA at 32.3% and 8.3% l_B are extrapolated. In addition, the critical point according to the strength analysis (GNIA, variant B)—where the design failure index $F_{I_d,IFF} = 1$ —is marked. The safety factors used are $\gamma_{mc, GNA + LBA} = 1.63$ and $\gamma_{mc, LBA} = 2.04$.

Table V. Evaluation of design buckling resistance due to bifurcation analysis.

Method	MoS (%)	SRF	z/l_B (%)	Failure element
LBA	-4.4	0.96	32.3	Suction side cap (SSC)
GNIA + LBA	7.5	1.09	32.3	Suction side cap (SSC)

A close to the design/characteristic load level (Figure 8). Notice that we extrapolated the curve for variant A (FF) for the last increments (dashed line). Both structural responses are non-linear and give a very different buckling resistance, 55.0% (variant A, FF) and 5.1% (variant B, FF) (Table IV). Variant B’s response, however, is more non-linear than variant A’s.

4.2.3. GL and Eurocode design resistance according to LBA and GNIA + LBA.

To compare the geometrically non-linear approach according to GL shown in the previous paragraph with the more simple linear approach (LBA described in Section 3.6.2), the results of the latter are shown in this paragraph. Also, we compare the linear approach according to GL with a geometrically non-LBA during the load path of the imperfect model recommended by Eurocode (GNIA + LBA described in Section 3.6.2).

A GNIA + LBA revealed two buckling modes (Figure 9). Those modes were in accordance with the two ‘decreasing’ modes of the perfect model in Figure 6. The difference was that the critical mode at design load was the same as the mode at failure ($P = P_{cr}$): 32.3% l_B . Notice that we extrapolated the curves 32.3% and 8.3% l_B for the last increments (dashed line in Figure 9) up to the point of instability. Comparing the resistance of the GNIA + LBA ($\gamma_{mc} = 1.63$) with the LBA ($\gamma_{mc} = 2.04$), we found that the LBA yields the lower result (Table V). Also, the design criterion was not successful for the LBA ($MoS = -4.4\%$). The investigated evaluation for the LBA is expressed in equation (29) and for the GNIA + LBA in equation (30). As well, the failure load of the design strength analysis ($MoS = -4.4\%$ w.r.t. P_d , variant B, IFF, Figure 8) is reached before buckling resistance due to GNIA + LBA. LBA and GNIA (variant B) using IFF revealed the same buckling resistance, when for both analyses, the design load level P_d is considered as load effect.

4.3. Introduction of imperfections

Since the application of the imperfections on the strength and stability resistance had a significant influence, we investigated two ways of introducing imperfections: (i) global scaling of the imperfection, where the dimple tolerance factor U_0 is varied, and (ii) local modification of the imperfection, where simply one dimple of a mode shape is applied in accordance with Eurocode’s recommendations.

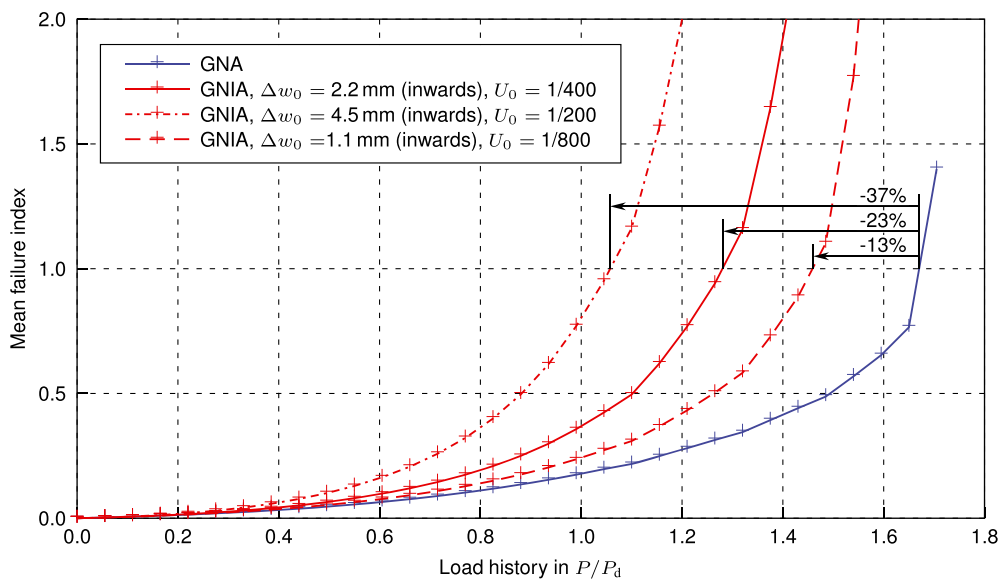


Figure 10. Different global scalings of mode shape imperfections with its largest dimple height of Δw_0 , oriented inwards to the blade. The dimple tolerance factor U_0 had a significant influence on the buckling resistance in terms of a geometrically non-linear strength analysis (GNIA).

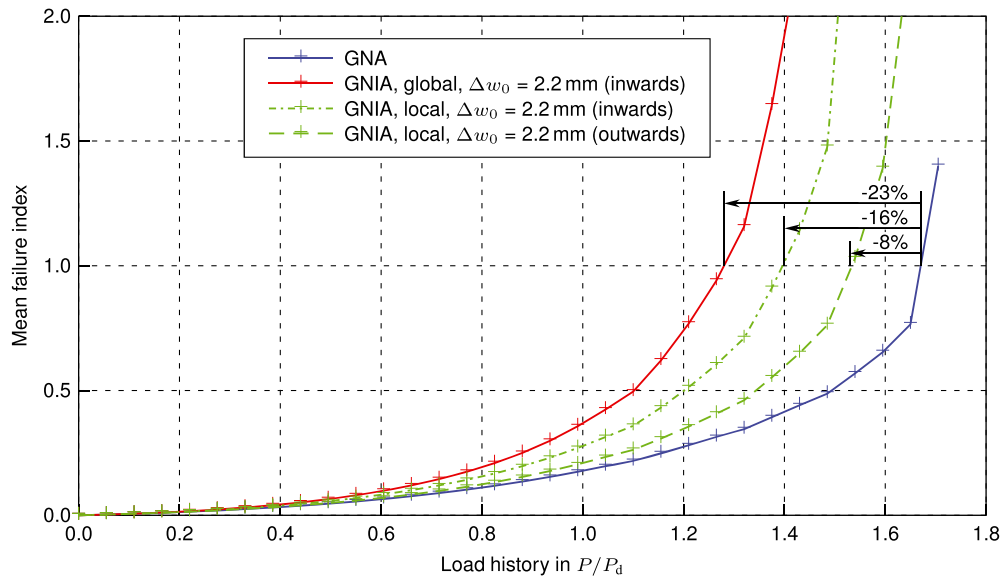


Figure 11. Local imperfection modifications oriented inwards and outwards.

4.3.1. Global scaling.

First, Tsai/Wu failure index (FI) was used to determine the load at failure. Then, we investigated the mean strength resistance by scaling (paragraph Imperfection in Section 3.6.2) the buckling mode shape at 32.3% blade length (Figure 5(a)) and found a significant influence of the applied dimple tolerance factor U_0 , which results in different initial dimple depths Δw_0 (Figure 10). For $\Delta w_0 = 1.1$ mm corresponding to $U_0 = 1/800$, the buckling resistance in terms of a geometrically non-linear strength analysis (GNIA) is decreased about 13% compared with the perfect model; for $\Delta w_0 = 2.2$ mm about 23%, and for $\Delta w_0 = 4.5$ mm about 37%.

4.3.2. Local modification.

According to Eurocode, parts of the imperfections can be excluded when they are unrealistic. In contrast to the previous paragraph, we only considered the maximum initial dimple of the mode shape at 32.2% blade length (Figure 5(a)) and found an increase of the strength resistance compared with the global scaling with a constant dimple tolerance factor $U_0 = 1/400$ (Figure 11).

5. DISCUSSION

5.1. Geometrically non-linear effects

The failure mechanism determined by a linear strength analysis (LA) using IFF seems unrealistic compared with the one revealed by a GNA (Table I). Thus, LA did not capture the highly non-linear response of the rotor blade structure as revealed by GNA and an ultimate full-scale test to failure.⁵

Considering the design strength resistance of the LA, FF is more critical than IFF (Table II). Considering the resistance of the GNA, however, IFF is more critical than FF, while the safety reserve between FF for GNA and LA is approximately the same. This leads to the conclusion that the geometrical non-linearities dominantly affect the transverse stresses of this particular blade design.

Safety factors and analysis concepts—based on experience from LA—cannot be expected to take non-linear effects correctly into account when the failure mechanism (buckling of the load-carrying cap and its location) and mode (IFF and FF) are not the same in both types of analysis. We discuss this statement in the following sections more detailed.

5.2. Evaluation of the blade design

5.2.1. GL guideline.

The conducted analyses according to the GL guideline are discussed in this paragraph. Table VI illustrates an overview of the results that we derived from the design strength and stability evaluation according to GL guideline shown in Sections 4.1 and 4.2. Comparison criterion is the margin of safety (MoS). The safety margin against instability using the GNA concepts

Table VI. Evaluation of the strength and stability limit states and their validation with an ultimate test to failure.

Method	Strength		Stability				Ultimate test to failure ⁵
	LA (IFF)*	LA (FF)*	LBA*	GNIA (A,FF) [†]	GNIA (B,FF) [†]	GNIA + LBA [‡]	Full-scale test
<i>MoS</i> (%)	154.0	122.7	−4.4	55.0	5.1	7.5	35.3

*Mandatory according to GL.

[†]Possible according to GL.

[‡]Possible according to Eurocode.

with imperfection (GNIA) is above design load for both: 55% for variant A and 5.1% for variant B. This large discrepancy is discussed later. An LBA yields an unsuccessful evaluation with an *MoS* of −4.4%. This can be justified by the linearized design load distribution assumed for this study, which is slightly above the target load (Figure 2). Regarding the evaluation of the strength, the safety using LA is 154.0% for IFF and 122.7% for FF. In comparison, a GNA (not recommended by GL) reveals an *MoS* of 55.1% for IFF and 73.1% for FF (Table II). The ultimate test to failure of the considered blade revealed an *MoS* of 35.3% above design load.⁵

That is, if the blade designer chooses the more realistic analysis method—a GNA—this specific blade design allows an additional safety margin of at least 9.9% comparing LBA as reference with the GNIA (variant B). Notice that the results of a GNIA were significantly driven by the dimple tolerance factor, which is responsible for the scaling of the eigenmode when the imperfection is applied to the model. We discuss this further in the next sections.

These facts show the need to spend more effort in determining a method for a geometrically non-linear evaluation of a wind turbine blade design, since the discrepancy between GL's GNIA variants itself and in comparison with an ultimate test to failure is still large; variant A is even 19.7% above the test, which is critical.

5.2.2. Eurocode.

In addition to the evaluation described earlier of the design according to GL, we investigated an approach recommended by Eurocode. For the evaluation of the stability limit state, Eurocode proposes a geometrically non-linear strength analysis combined with an LBA (GNIA + LBA) during the load path. We applied the imperfection as described in GL guideline. The lowest resistance—either due to buckling or due to IFF—is considered for evaluation. Considering Table VI, the GNIA + LBA yields an *MoS* of 7.5%, whereas the GNIA (variant B) yields IFF already at −4.4% as illustrated in Figure 9. Thus, the design evaluation using GNIA + LBA plus GL's IFF analysis philosophy would not pass the requirements according to Eurocode.

5.2.3. Variant A versus variant B.

Germanischer Lloyd's simplified approach (variant A) is around 50% more optimistic than variant B (Table IV). This is a large difference caused by the reduction of the moduli in variant B. For this particular blade design, this leads to a more flexible model that is prone to buckle earlier and causes a large difference in the *MoS* between variants A and B. The presumption by GL, that the difference between variants A and B is negligible, contradicts with the investigations made in this study. Since the stability analysis is conducted as strength analysis, we would prefer variant A because the application of the safety factors on the moduli makes more sense when conducting a bifurcation analysis. Such a large deviation of the moduli is not expected.

5.2.4. Critical failure mode in GNIA.

Germanischer Lloyd considers an FF evaluation in the GNIA, which might be based on the assumption that FF was more critical than IFF when an LA was used (Table II). The GNIA (Table IV) conducted for this particular blade design, however, shows that IFF was more critical than FF, leading to an *MoS* of 23.5% for variant A and 2.9% for variant B. Evaluation based on a GNIA using IFF still allows an additional safety margin of about 7–28% for the designer when the LBA is used as reference. To clarify that the failure mode discrepancy is based on geometrically non-linear effects, we observed the failure mechanism seen in our simulations and the full-scale test: the load-carrying cap deflected inwards mainly because of buckling (Figure 7(a)), which caused high transverse stresses in the first inner uniaxial layer leading to cracks parallel to the fibres, either in the matrix or in the fibre–matrix interface. Eventually, this mechanism leads to ultimate failure. To conclude, IFF is not required by GL but is the governing failure mode for this particular blade.

Notice that the characteristic load considered for IFF analysis was determined by the assumption that the load envelope consisted of abnormal load cases (Section 3.3). When normal load cases were considered, the *MoS*s of the GNIA (Table IV) would be larger.

5.3. Safety factors

For this particular blade design, the *MoS* of 23.5% determined by a GNIA (variant A) using IFF (Table IV) seems to be at a realistic and sufficient level compared with the full-scale test to failure (Table VI). This has also been proven by the blade's successful operation in the field. The GNIA also captured the realistic failure mechanism, but there is still a safety margin left. Therefore, the safety factors combined with the size of the imperfection proposed by GL—when using a non-linear approach—may be too conservative, but more studies are required to conclude this.

The safety factor C_{3c} , which takes the inaccuracy of a linear stability analysis into account, was verified with a GNIA + LBA (Table V). GNIA + LBA's stability resistance is underestimated by 8.9%. Thus, the quantity of C_{3c} is conservative but seems to include a relatively large safety margin for this particular blade design.

Validating the computationally derived limit state resistance with the ultimate test to failure (conducted after the static and fatigue certification tests)—disregarding non-LA concepts—the divergence is large (LBA versus test in Table VI). A reason for this large range seems to be the high material safety factor for stability in the GL guideline.

5.4. Introduction of imperfections

5.4.1. Global scaling.

The method proposed by GL to apply the imperfection is adopted from Eurocode. Considering steel structures, Schneider³⁰ states that pre-deforming a model using the first eigenmode as imperfection is a good approach for structures whose response is geometrically non-linear dominated and not materially non-linear. But the dimple tolerance factor proposed in Eurocode is 10 times higher than the factor proposed by GL ($U_{0,Eurocode} = 1/40$ vs $U_{0,GL} = 1/400$), which can to some extent be explained by the different materials: steel and fibre-reinforced plastics. The aforementioned facts justify the method used in GL guideline with the exception of the dimple tolerance factor, which might be a rule of thumb. The results of the variation of the dimple tolerance factor show that the impact on the stability resistance is significant (Figure 10). Regarding the qualitative difference between a linear and a non-linear stability analysis, we suggest to seek for a method to determine a reasonable dimple tolerance factor.

5.4.2. Local modification.

Eurocode states to exclude unrealistic imperfections. When we applied merely the first critical buckle of the mode shape, the resistance was larger compared with a globally applied imperfection. Figure 7(a) illustrates the affected regions when the mode shape was applied globally. Applying merely a simple dimple, the resistance was 9% higher. This is because the structure is not pre-deformed to the extent wherein it is more sensitive to buckling. We confirmed Eurocode's recommendation¹⁵ that the critical dimple should be directed to the curvature centre—inwards to the blade. Since the GNIA was very sensitive to the applied dimple tolerance factor as shown in Section 4.3 and the local modification was different from the global scaling as well, we suggest to seek for a more realistic way to model geometrical imperfections on wind turbine blades. A mathematical approach for composite structures is presented by Lindgaard *et al.*³¹

5.5. Model

The model used in this study was based on 3D composite brick elements. Therefore, we had to exclude tapered elements, since they were not properly modelled. More accurate wind turbine blade modelling techniques consisting of a mix of shell and solid elements are discussed by Fedorov *et al.*³²

Since the considered blade shows a highly geometrically non-linear response, a non-linear material model, such as proposed by Philippidis and Antoniou,³³ could improve the capability of the FE model. To obtain a more detailed insight of the failure mode (IFF or interlaminar shear), action-plane criterions can be applied, such as proposed by Puck.²⁰

6. CONCLUSIONS

A geometrically non-linear structural response of a 34 m wind turbine blade under flap-wise loading has been compared with an LA. A linear strength analysis did not capture the critical areas, the failure mechanism and the failure mode as revealed by an ultimate test to failure and a GNA. Using a GNIA to evaluate the design, however, revealed a realistic failure mechanism and the critical mode.

Further focus was on determining the mean and design resistance in the ultimate strength and stability limit states. For the design resistance, we used LAs according to the least stringent GL requirements and compared the results with non-linear approaches proposed by GL and Eurocode, which require the application of an imperfection.

An LBA according to the least stringent GL requirements yielded more conservative results than the geometrically non-linear approaches proposed by GL. Consequently, the investigated blade designed after the lesser requirements was sufficient. Using the non-linear approaches, considering IFF as the critical failure mode, yielded still a significant safety margin for the designer (7–28%).

One of the GL's geometrically non-linear concepts requires the application of the safety factors on the moduli (variant B). This method seems unrealistic because it can trigger unrealistic instabilities and therefore predict failure at too low load level, at least for instability-sensitive blades. In another GL concept (variant A), the blade strength is overestimated compared with the full-scale test, which is critical. GL, however, requires merely the consideration of FF in the non-LA. Thus, important failure mechanisms may be overlooked as shown for this particular blade.

The non-linear Eurocode approach—a bifurcation analysis during the load path—revealed a higher stability resistance than GL's LBA.

We found that the non-linear structural response was significantly dependent on the scaling of an applied imperfection. The way to apply an imperfection according to Eurocode appears to be more realistic compared with the GL approach.

Since the considered blade withstood 135% of the design load at an ultimate full-scale test to failure and the blade has proven to operate successfully in the field, GL's safety factors combined with the size of the imperfection, when using a non-linear approach, may be too conservative. Therefore, we suggest to spend more effort in gaining an approach that contains a more realistic GNIA. Experimental investigations are required to superiorly understand the behaviour of imperfect wind turbine sub-components. We believe that more focus should be spent on a reasonable scaling factor of the imperfection and the derivation of the most realistic imperfection.

ACKNOWLEDGEMENTS

The work presented in this paper was partly supported by the Danish Energy Agency through the Energy Technology Development and Demonstration Program (EUDP 2010), grant no. 64011-0006. The supported project is named Experimental Blade Research Phase 2, and the financial support was greatly appreciated. Further, this study was funded by the PROMOS scholarship of the German Academic Exchange Service (DAAD).

APPENDIX

Tsai/Wu criterion Using the nomenclature according to VDI 2014,²¹ the global Tsai/Wu criterion is defined as follows:

$$F_1\sigma_1 + F_2\sigma_2 + F_3\sigma_3 + F_{11}\sigma_1^2 + F_{22}\sigma_2^2 + F_{33}\sigma_3^2 + F_{44}\tau_{23}^2 + F_{55}\tau_{31}^2 + F_{66}\tau_{21}^2 + 2F_{12}\sigma_1\sigma_2 + 2F_{23}\sigma_2\sigma_3 + F_{13}\sigma_1\sigma_3 \leq 1 \quad (31)$$

where

$$F_1 = \frac{1}{R_{\parallel}^t} - \frac{1}{R_{\parallel}^c} \quad (32)$$

$$F_2 = F_3 = \frac{1}{R_{\perp}^t} - \frac{1}{R_{\perp}^c} \quad (33)$$

$$F_{11} = \frac{1}{R_{\parallel}^t R_{\parallel}^c} \quad (34)$$

$$F_{22} = F_{33} = \frac{1}{R_{\perp}^t R_{\perp}^c} \quad (35)$$

$$F_{44} = \frac{1}{R_{\perp\perp}^2} \quad (36)$$

$$F_{55} = F_{66} = \frac{1}{R_{\perp\parallel}^2} \quad (37)$$

Moreover, F_{23} , F_{12} and F_{13} are interaction terms set according to measurements.

Puck/Knaust criterion for IFF The Puck/Knaust criterion for IFF is defined as follows:

$$F_{22}(\sigma_2^2 + \sigma_3^2 - \sigma_2\sigma_3 + 3\tau_{23}^2) + F_2(\sigma_2 + \sigma_3) + F_{55}(\tau_{21}^2 + \tau_{31}^2) + \frac{\sigma_1^2}{R_{\parallel\text{IFF}}^t R_{\parallel\text{IFF}}^c} + \left(\frac{1}{R_{\parallel\text{IFF}}^t} - \frac{1}{R_{\parallel\text{IFF}}^c}\right)\sigma_1 \leq 1 \quad (38)$$

FF condition for uniaxial laminae The following very simple fracture condition for FF in tension and compression of an uniaxial laminae is, respectively, as follows:

$$\frac{\sigma_1}{R_{\parallel}^t} \leq 1 \quad \text{for } \sigma_1 > 0 \quad (39)$$

and

$$\frac{\sigma_1}{-R_{\parallel}^c} \leq 1 \quad \text{for } \sigma_1 < 0 \quad (40)$$

Tsai/Wu modifications to obtain FF and IFF results according to Puck/Knaust To obtain FF and IFF according to Puck/Knaust, the following modifications in the Tsai/Wu criterion are required. With the stress product $\sigma_1\sigma_2$ and $\sigma_1\sigma_3$, the coefficients F_{12} and F_{13} are set to zero:

$$2 \cdot F_{12} = 2 \cdot F_{13} = 0 \quad (41)$$

To obtain FF, all non-fibre-oriented strengths (R_{\perp}^t , R_{\perp}^c , $R_{\perp\parallel}$ and $R_{\perp\perp}$) are set to unrealistic high values (i.e. 10^4 N mm^{-2}). In this way, approximately the same results may be obtained as from the FF conditions in accordance with equations (39) and (40).

To obtain IFF, the inter-fibre strength in fibre direction is calculated by

$$R_{\parallel\text{IFF}}^t = (1.3 \dots 1.5) R_{\parallel}^t \quad (42)$$

and

$$R_{\parallel\text{IFF}}^c = (1.3 \dots 1.5) R_{\parallel}^c \quad (43)$$

Further, the coefficients F_{11} , F_1 , F_{44} and F_{23} are modified. The coefficients F_{11} and F_1 for σ_1^2 and σ_1 are calculated as follows:

$$F_{11} = \frac{1}{R_{\parallel\text{IFF}}^t R_{\parallel\text{IFF}}^c} \quad (44)$$

and

$$F_1 = \frac{1}{R_{\parallel\text{IFF}}^t} - \frac{1}{R_{\parallel\text{IFF}}^c} \quad (45)$$

The coefficient F_{44} for τ_{23}^2 is calculated as follows:

$$F_{44} = 3F_{22} \quad (46)$$

The coefficient F_{23} for the product of $\sigma_2\sigma_3$ is calculated as follows:

$$F_{23} = -\frac{F_{22}}{2} \quad (47)$$

REFERENCES

1. Brazier L. On the flexure of thin cylindrical shells and other 'thin' sections. *Proceedings of the Royal Society of London* 1927; **Series A 116**: 104–114.
2. Cecchini LS, Weaver PM. Brazier effect in multibay airfoil sections. *AIAA Journal* 2005; **43**: 2252–2258.
3. Jensen FM, Puri AS, Dear JP, Branner K, Morris A. Investigating the impact of non-linear geometrical effects on wind turbine blade - part 1: current issues and future challenges in design optimisation. *Wind Energy* 2011; **14**: 239–254. DOI: 10.1002/we.415.

4. Kong C, Bang J, Sugiyama Y. Structural investigation of composite wind turbine blade considering various load cases and fatigue life. *Energy* 2005; **30**: 2101–2114. DOI: 10.1016/j.energy.2004.08.016.
5. Jensen FM, Falzon BG, Ankersen J, Stang H. Structural testing and numerical simulation of a 34m composite wind turbine blade. *Composite Structures* 2006; **76**: 52–61.
6. Jørgensen ER, Borum KK, McGugan M, Thomsen CL, Jensen FM, Debel CP, Sørensen BF. Full scale testing of wind turbine blade to failure - flapwise loading. Forskningscenter Risø. Risø-R; No. 1392(EN), Denmark, 2004.
7. Overgaard LCT, Lund E, Thomsen OT. Structural collapse of a wind turbine blade. Part A: static test and equivalent single layered models. *Composites Part A: Applied Science and Manufacturing* 2010; **41**: 257–270.
8. Overgaard LCT, Lund E. Structural collapse of a wind turbine blade. Part B: progressive interlaminar failure models. *Composites Part A: Applied Science and Manufacturing* 2010; **41**: 271–283.
9. Yang J, Peng C, Xiao J, Zeng J, Xing S, Jin J, Deng H. Structural investigation of composite wind turbine blade considering structural collapse in full-scale static tests. *Composite Structures* 2013; **97**: 15–29.
10. Chen X, Zhao W, Zhao XL, Xu JZ. Failure test and finite element simulation of a large wind turbine composite blade under static loading. *Energies* 2014; **7**: 2274–2297.
11. Eder MA, Bitsche R, Nielsen M, Branner K. A practical approach to fracture analysis at the trailing edge of wind turbine rotor blades. *Wind Energy* 2014; **17**: 483–497. DOI: 10.1002/we.1591.
12. Eder MA, Bitsche R. Fracture analysis of adhesive joints in wind turbine blades. *Wind Energy* 2014; **18**: 1007–1022, DOI: 10.1002/we.1744.
13. GL. Guideline for the certification of wind turbines. Germanischer Lloyd Industrial Services, Hamburg, Germany, 2010.
14. Thompson JMT. Optimization as a generator of structural instability. *International Journal of Mechanical Sciences* 1972; **14**: 627–629.
15. CEN. Eurocode 3: design of steel structures - part 1–6: strength and stability of shell structures; EN 1993-1-6:2007 + AC:2009. European Committee for Standardization, 2009.
16. ISO. ISO 2394 - general principles on reliability for structures. International Organization for Standardization, 1998.
17. IEC. IEC 61400-1 - wind turbines - part 1: design requirements for wind turbines. International Electrotechnical Commission, 2005.
18. IEC. IEC 61400-23 - wind turbines - part 23: full-scale structural testing of rotor blades. International Electrotechnical Commission, 2014.
19. Tsai SW, Wu EM. A general theory of strength for anisotropic materials. *Journal of Composite Materials* 1971; **5**: 58–80.
20. Puck A. Festigkeitsanalyse von Faser-Matrix-Laminaten: Modelle für die Praxis. Hanser München, 1996.
21. VDI. VDI 2204 - part 3 - development of FRP components (fibre-reinforced plastics) - analysis. Verein Deutscher Ingenieure, 2006.
22. Puck A. Praxisgerechte Bruchkriterien für hochbeanspruchte Faser-Kunststoff-Verbunde. *Kunststoffe, Hanser München* 1992; **82**: 149–155.
23. MSC. Marc 2008 r1 - volume B: element library. MSC Software Corporation, 2008.
24. Rosemeier M. Non-linear ultimate limit state analysis of a wind turbine blade. *MSc Thesis*, DTU Wind Energy, 2013.
25. Thomsen LC, Eisenberg PJ. Risø-1-2083(EN) - blade test SSP34#2 edgewise and flapwise - final static test. Risø National Laboratory, Denmark, 2003.
26. Vel SS, Caccese V, Zhao H. Modeling and analysis of tapered sandwich beams. In *Proceedings of the American Society for Composites, Seventeenth Technical Conference*. CRC Press: London, 2002.
27. MSC. Marc 2008 r1 - volume C: program input. MSC Software Corporation, 2008.
28. GL. List of certifications - rotor blades. Germanischer Lloyd Industrial Services, Hamburg, Germany, 2012.
29. MSC. Marc 2008 r1 - volume A: theory and user information. MSC Software Corporation, 2008.
30. Schneider W, Timmel I, Höhn K. The conception of quasi-collapse-affine imperfections: a new approach to unfavourable imperfections of thin-walled shell structures. *Thin-walled Structures* 2005; **43**: 1202–1224.
31. Lindgaard E, Lund E, Rasmussen K. Nonlinear buckling optimization of composite structures considering ‘worst’ shape imperfections. *International Journal of Solids and Structures* 2010; **47**: 3186–3202.
32. Fedorov V, Berggreen C, Krenk S, Branner K. Bend-twist coupling effects in wind turbine blades. *PhD Thesis*, DTU Wind Energy, 2012.
33. Philippidis TP, Antoniou EA. A progressive damage FEA model for glass/epoxy shell structures. *Journal of Composite Materials* 2013; **47**: 623–637.